Analysis of a novel 3C-SiC thin layer on silicon diaphragms for enhanced stress amplification in MEMS piezoresistive pressure sensors

**Nguyen Chi Cuong*, Trinh Xuan Thang, Lam Minh Thinh, Vuong Dinh Duy Phuc,
Truong Huu Ly, Ngo Vo Ke Thanh, Le Quoc Cuong**

Research Laboratories of Saigon High-Tech-Park, Lot I3, N2 Street, Saigon High-Tech-Park, District 9, Ho Chi Minh City, Vietnam

Abstract:

This study analyses the square diaphragm structure of a micro-electro-mechanical system (MEMS) pressure sensor using the finite element method (FEM). The research investigates an enhancement in stress distribution achieved by coating a silicon (Si) diaphragm with a thin layer of silicon carbide (3C-SiC). Applying a thin layer of 3C-SiC material onto a Si diaphragm enhances the stress distribution of MEMS pressure sensors. The design structure of the square diaphragm of a MEMS pressure sensor is simulated and analysed using 3D FEM in COMSOL multiphysics. Four piezo-resistors are configured in a Wheatstone bridge to translate resistance variations into an output voltage. Then, the stress distributions are calculated by solving the 3D structures of MEMS pressure sensors in the stationary solver of the solid mechanics module in COMSOL multiphysics. The findings indicate a significantly higher stress distribution in the 3C-SiC layer compared to a solely silicon diaphragm. Consequently, it is posited that the stress distribution in MEMS pressure sensors could be considerably augmented with increasing pressure, increasing diaphragm length, and decreasing diaphragm thickness. Also, the output voltage of more than 20 mV can be achievable with this design for using the thin layer of 3C-SiC material on a Si diaphragm in designing MEMS piezoresistive pressure sensors.

1. Introduction

Pressure sensors are extensively utilised in various technical applications including medical [1], automotive [2], wearable devices [3], and aerospace sectors [4]. Micro-electro-mechanical systems (MEMS) pressure sensors offer numerous advantages, such as compact size, reduced power consumption, high sensitivity, and linearity [1]. Based on their working principles, pressure sensors can be categorised into piezoresistive [5-7], capacitive [8], optical fibre [9], resonant [10], and piezoelectric types [11]. For the enhancement of stress amplification, sensitivity, and linearity in MEMS pressure sensors, piezoresistivity [5, 6] is favoured. This involves converting the applied pressure signal into an electrical output signal, i.e., resistance, to measure the stress states in materials. An increase in material stress amplification leads to heightened sensitivity in MEMS pressure sensors.

Various electrical materials' piezoresistive properties are explored to measure stress states in materials [12]. Literature reviews suggest that conventional piezoresistive sensors, constructed using metal films (such as Au [13], Cu [14], Mn [15]), alloy films (like Bi-Sb [16]), and cermet films (such as Au-glass [17], RuO_2 [18]), exhibit limited sensitivity, substantial temperature dependence, and high power consumption. Consequently, metal strain sensors have been substituted by semiconducting materials like silicon (Si) [19, 20], polysilicon (Poly-Si) [21], silicon carbide (3C-SiC) [22, 23], graphene [24], and diamond [25], enhancing the stress distribution and sensitivity of MEMS piezoresistive pressure sensors. Silicon carbide (3C-SiC) is particularly suited for MEMS piezoresistive pressure sensors in harsh environmental conditions due to its wide bandgap, corrosion resistance, excellent chemical inertness, and high Young's modulus. Recently, MEMS silicon carbide (SiC) pressure sensors have been operational under high pressure and high-temperature conditions, where conventional silicon sensors are ineffective [26-29]. The use of square diaphragms made of SiC materials, which show greater stress distribution, can lead to higher sensitivity in MEMS piezoresistive pressure sensors [30, 31]. However, the combination of a thin 3C-SiC layer on a Si diaphragm (3C-SiC/Si wafer) has not been previously explored for enhancing the stress distribution in MEMS piezoresistive pressure sensors.

This study investigates the application of a 3C-SiC layer on a Si diaphragm to achieve higher stress amplification

*Corresponding author: Email: cuong.nguyenchi@shtplabs.org

and robust performance in MEMS piezoresistive pressure sensors. A square-shaped diaphragm of a MEMS pressure sensor is modelled using the finite element method (FEM) in COMSOL multiphysics [32] to calculate its stress states. A thin layer of silicon carbide (3C-SiC) is applied atop a (100) plane Si wafer to augment the diaphragm's stress. Subsequently, four piezoresistors, configured in a Wheatstone bridge, are employed to translate resistance variations into the output voltage. The resulting output voltage from the 3C-SiC on the Si square diaphragm is then evaluated across a broad spectrum of pressure (p) and diaphragm dimensions.

2. Materials and methods

2.1. Stress-strain relations for single crystal Si and SiC materials

To examine the linear elastic behaviour of orthotropic and homogeneous materials, such as silicon (Si) and silicon carbide (SiC), it is essential to understand how an external force acting upon a solid body generates internal forces that cause deformation, stress, and strain. Fig. 1 illustrates the stress components within a small segment of a solid body.
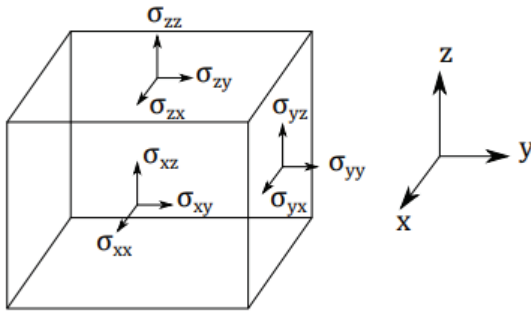

Fig. 1. Stress components in a small cubic element of a material. Variables σ_{xx}, σ_{yy}, σ_{zz} are the normal stress components in the x, y, and z direction, respectively. Variables σ_{xy}, σ_{xz}, σ_{yz} represent the shear stress components in the x, y, and z direction, respectively.

A linear relationship between stress and strain is established by Hooke's Law [33], as shown in Eq. (1):

$$
\begin{bmatrix} \sigma_{xx} \\ \sigma_{yy} \\ \sigma_{zz} \\ \sigma_{yz} \\ \sigma_{xz} \\ \sigma_{xy} \end{bmatrix} = \hat{E} \begin{bmatrix} 1-v & v & v & 0 & 0 & 0 \\ v & 1-v & v & 0 & 0 & 0 \\ v & v & 1-v & 0 & 0 & 0 \\ 0 & 0 & 0 & \frac{1-2v}{2} & 0 & 0 \\ 0 & 0 & 0 & 0 & \frac{1-2v}{2} & 0 \\ 0 & 0 & 0 & 0 & 0 & \frac{1-2v}{2} \end{bmatrix} \begin{bmatrix} \varepsilon_{xx} \\ \varepsilon_{yy} \\ \varepsilon_{zz} \\ 2\varepsilon_{yz} \\ 2\varepsilon_{xz} \\ 2\varepsilon_{xy} \end{bmatrix} - \frac{E\alpha\Delta T}{1-2v}\begin{bmatrix} 1 \\ 1 \\ 1 \\ 0 \\ 0 \\ 0 \end{bmatrix} \quad (1)
$$

where $\hat{E} = \frac{E}{(1+v)(1-2v)}$, E and v are Young's modulus and Poisson's ratio of the material, respectively, α is the

coefficient of thermal expansion, and ΔT is the change in temperature of the solid, ε_{xx}, ε_{yy}, ε_{zz} are the normal strain components in the x, y, and z directions, respectively, and ε_{xy}, ε_{xz}, ε_{yz} are the shear strain components in x, y, and z directions, respectively.

Considering that a thin plate is only subjected to load forces in the x-y directions, the plane stress assumption ($\sigma_{yz}=\sigma_{xz}=\sigma_{zz}=0$) is applied. Therefore, the stress components in Eq. (1) are simplified as shown in Eq. (2):

$$
\begin{bmatrix} \sigma_{xx} \\ \sigma_{yy} \\ \sigma_{xy} \end{bmatrix} = \frac{E}{1-v^2}\begin{bmatrix} 1 & v & 0 \\ v & 1 & 0 \\ 0 & 0 & \frac{1-v}{2} \end{bmatrix}\begin{bmatrix} \varepsilon_{xx} \\ \varepsilon_{yy} \\ 2\varepsilon_{xy} \end{bmatrix} - \frac{E\alpha\Delta T}{1-v}\begin{bmatrix} 1 \\ 1 \\ 0 \end{bmatrix} \quad (2)
$$

Si and SiC are known to be anisotropic materials [34-36]. Thus, the relationship between stress and strain for these materials, considering their anisotropic coefficients, can be generally expressed as shown in Eq. (3):

$$
\begin{bmatrix} \sigma_{xx} \\ \sigma_{yy} \\ \sigma_{zz} \\ \sigma_{yz} \\ \sigma_{xz} \\ \sigma_{xy} \end{bmatrix} = \begin{bmatrix} C_{11} & C_{12} & C_{12} & 0 & 0 & 0 \\ C_{12} & C_{11} & C_{12} & 0 & 0 & 0 \\ C_{12} & C_{12} & C_{11} & 0 & 0 & 0 \\ 0 & 0 & 0 & C_{44} & 0 & 0 \\ 0 & 0 & 0 & 0 & C_{44} & 0 \\ 0 & 0 & 0 & 0 & 0 & C_{44} \end{bmatrix}\begin{bmatrix} \varepsilon_{xx} \\ \varepsilon_{yy} \\ \varepsilon_{zz} \\ \varepsilon_{yz} \\ \varepsilon_{xz} \\ \varepsilon_{xy} \end{bmatrix} \quad (3)
$$

where C_{11}, C_{12}, and C_{44} are components in a 6x6 matrix, often referred to as the coefficients of elasticity for anisotropic materials.

The specific stress-strain relationship for anisotropic Si in the <100> direction on a (100) plane Si wafer is expressed in Eq. (4) [33]:

$$
\begin{bmatrix} \sigma_{xx} \\ \sigma_{yy} \\ \sigma_{zz} \\ \sigma_{yz} \\ \sigma_{xz} \\ \sigma_{xy} \end{bmatrix} = \begin{bmatrix} 165.7 & 63.9 & 63.9 & 0 & 0 & 0 \\ 63.9 & 165.7 & 63.9 & 0 & 0 & 0 \\ 63.9 & 63.9 & 165.7 & 0 & 0 & 0 \\ 0 & 0 & 0 & 79.6 & 0 & 0 \\ 0 & 0 & 0 & 0 & 79.6 & 0 \\ 0 & 0 & 0 & 0 & 0 & 79.6 \end{bmatrix}\begin{bmatrix} \varepsilon_{xx} \\ \varepsilon_{yy} \\ \varepsilon_{zz} \\ \varepsilon_{yz} \\ \varepsilon_{xz} \\ \varepsilon_{xy} \end{bmatrix} \text{[GPa] (4)}
$$

Similarly, for anisotropic 3C-SiC in the <100> direction on a (100) plane Si wafer, the relationship is given in Eq. (5) [36, 37]:

$$
\begin{bmatrix} \sigma_{xx} \\ \sigma_{yy} \\ \sigma_{zz} \\ \sigma_{yz} \\ \sigma_{xz} \\ \sigma_{xy} \end{bmatrix} = \begin{bmatrix} 395 & 132 & 132 & 0 & 0 & 0 \\ 132 & 395 & 132 & 0 & 0 & 0 \\ 132 & 132 & 395 & 0 & 0 & 0 \\ 0 & 0 & 0 & 236 & 0 & 0 \\ 0 & 0 & 0 & 0 & 236 & 0 \\ 0 & 0 & 0 & 0 & 0 & 236 \end{bmatrix}\begin{bmatrix} \varepsilon_{xx} \\ \varepsilon_{yy} \\ \varepsilon_{zz} \\ \varepsilon_{yz} \\ \varepsilon_{xz} \\ \varepsilon_{xy} \end{bmatrix} \text{[GPa] (5)}
$$

Table 1 lists the Young's modulus (E), shear modulus (G), Poisson's ratio (ν), and mass density (ρ) of Si and 3C-SiC materials in the (100) plane Si wafer. These values are incorporated in the finite element method (FEM) in COMSOL multiphysics [32] for calculating the stress and strain of Si and 3C-SiC diaphragms in MEMS pressure sensors.

Table 1. The mechanical properties of silicon (Si) and silicon carbide (SiC) in the <100> orientation on the (100) plane of an Si wafer [35-37].

Materials	Orientation	Young's modulus (GPa)	Shear modulus (GPa)	Poisson's ratio	Mass density (kg/m³)
Si	<100>	129.8	79.5	0.278	2330
3C-SiC	<100>	395	236	0.25	3210

For calculating stress and strain in homogeneous anisotropic materials like Si and 3C-SiC, solutions to the system equations of Eq. (1) are provided for 3D problems without body force, applied load, and boundary conditions. However, to simulate the complex structure of MEMS pressure sensors, FEM is required, incorporating specific boundary conditions such as applied pressure (p) and clamped boundaries. After solving, the stress and strain distributions in MEMS pressure sensors can be evaluated.

2.2. Piezoresistive effect for single crystal Si and SiC materials

Figure 2 demonstrates the alignment of all piezoresistors in the n-type SiC/p-type Si diaphragm. These are arranged in a rotated square diaphragm at 45° for the <100> crystallographic orientation, which has the highest piezoresistive gauge factors for n-type SiC [36]. The change in resistivity of the piezoresistive sensing element is given by:

$$\frac{\Delta\rho}{\rho} = \frac{\Delta R}{R} = \pi_l \sigma_l + \pi_t \sigma_t = \pi_{11}\sigma_l + \pi_{12}\sigma_t \qquad (6)$$

where ρ is the resistivity of the material, R is the resistance of the material, σ_l and σ_t are the longitudinal and transverse stresses in the piezoresistors, respectively, π_l and π_t are the longitudinal and transverse piezoresistive coefficients, respectively, and π_{11} and π_{12} are the fundamental piezoresistive coefficients of the single crystal 3C-SiC and Si materials [33, 34].

Table 2. The piezoresistive coefficients (π_{11}, π_{12}, π_{44}) in the <100> direction of (100) silicon (Si) [35].

Resistivity, ρ	π_{11} (10^{-11}/Pa)	π_{12} (10^{-11}/Pa)	π_{44} (10^{-11}/Pa)
p-Si (7.8 Ω.cm)	6.6	-1.1	-138.1
n-Si (11.7 Ω.cm)	-102.2	53.4	-13.6

Table 3. The piezoresistive coefficients (π_{11}, π_{12}, π_{44}) in direction <100> of (100) silicon carbide (3C-SiC) [34, 35].

Resistivity, ρ	π_{11} (10^{-11}/Pa)	π_{12} (10^{-11}/Pa)	π_{44} (10^{-11}/Pa)
p-3C-SiC (0.14 Ω.cm)	1.5	-1.4	18.1
n-3C-SiC (0.7 Ω.cm)	-9.6	5.8	1.6

For the design of the sensing element, the opposing signs of π_{11} and π_{12}, as presented in Tables 2 and 3, suggest that it is advantageous to maximise the longitudinal stress (σ_l) while minimising the transverse stress (σ_t). This approach facilitates a more significant change in the resistance (ΔR) of the piezoresistors. Consequently, the sensing elements are subjected to a simple uniaxial loading beam along the longitudinal axis. Under these conditions, only the longitudinal stress component σ_l is considered, and the transverse stress component σ_t is disregarded. Thus, Eq. (6) can be simplified to Eq. (7):

$$\frac{\Delta\rho}{\rho} = \frac{\Delta R}{R} = \pi_l \sigma_l = \pi_{11}\sigma_l \qquad (7)$$

This simplification underscores that the resistance of the sensing elements will increase under compressive stress (indicated by a positive sign) and decrease under tensile stress (indicated by a negative sign). This relationship between stress and resistance change is crucial for the effective functioning of the sensing elements in piezoresistive applications.
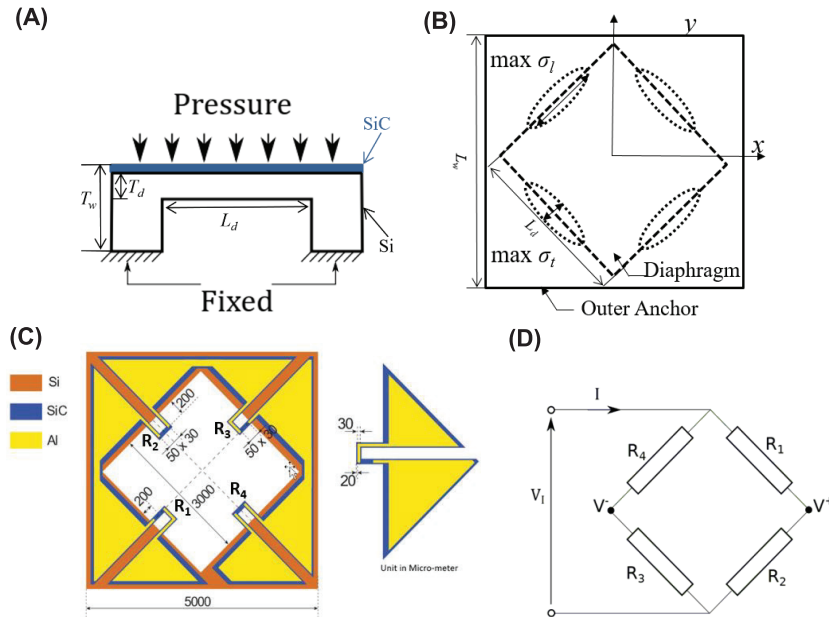

Fig. 2. (A) Schematic of the working principle of the device; (B) top-down view of maximum distributed stresses; (C) arrangement of the four piezoresistors; and (D) circuit diagram of resistors in full Wheatstone bridge forming the square diaphragm of the MEMS piezoresistive pressure sensors.

2.3. Sensor design and working principles

As depicted in Fig. 2A, a thin square diaphragm is supported by a thick Si substrate. A rotated square diaphragm of 45 degrees is proposed to maximise sensitivity, designed for the <100> direction on a (100) plane n-type 3C-SiC/p-type Si wafer. Additionally, a thin layer of 3C-SiC (approximately 500 nm) is applied on top of the Si diaphragm to enhance its stress distribution, as shown in Fig. 2A. Upon the application of pressure (*p*) to the diaphragm, stress concentrates at the corners of the thin SiC on Si diaphragm. This results in maximum distributed stresses (σ_l and σ_t) along the edges of the diaphragm and the substrate of the MEMS pressure sensor, as illustrated in Fig. 2B. Fig. 2C displays the placement of four piezoresistors (R_1, R_2, R_3, R_4) at these points of maximum stress on the diaphragm. When pressure is applied to the sensor diaphragm, the pairs of piezoresistors (R_1, R_3) and (R_2, R_4) undergo an equal and opposite change in resistance [35]. Subsequently, the piezoresistors R_1, R_2, R_3, and R_4 are interconnected in a Wheatstone bridge formation, as shown in Fig. 2D, to transform the resistance changes into an output voltage. The output voltage (V_{out}) of the Wheatstone bridge, resulting from bridge unbalance, is given by Eq. (8):

$$V_{out} = V^+ - V^- = \frac{R_1 R_3 - R_2 R_4}{(R_1 + R_2)(R_3 + R_4)} V_I \qquad (8)$$

where V_{out} is the output voltage and V_I is the source voltage.

When R_1 and R_3 experience stress, their relative change in resistance is given by:

$$\frac{\Delta R_1}{R_1} = \frac{\Delta R_3}{R_3} = \pi_l \sigma_{l_1} + \pi_t \sigma_{t_1} = 0 + \pi_t \sigma_{t_1} = \alpha_1 \qquad (9)$$

where $\sigma_{l_1} (= \sigma_{xy})$ and $\sigma_{t_1} (\approx -\sigma_{xy})$ are the longitudinal and transverse stress components at the locations of R_1 or R_3, respectively.

Similarly, the relative change in resistance for R_2 and R_4 is given by:

$$\frac{\Delta R_2}{R_2} = \frac{\Delta R_4}{R_4} = \pi_l \sigma_{l_2} + \pi_t \sigma_{t_2} = \pi_l \sigma_{l_2} + 0 = -\alpha_2 \qquad (10)$$

where $\sigma_{l_2} (= \sigma_{xy})$ and $\sigma_{t_2} (\approx -\sigma_{xy})$ are the longitudinal and transverse stress components taken at the locations of R_2 or R_4, respectively.

The relative change of voltage at the bridge output (or bridge sensitivity) can be rewritten as:

$$\frac{\Delta V}{V} = \frac{\alpha_1 + \alpha_2}{2 + \alpha_1 - \alpha_2} \qquad (11)$$

Since the quantity $\alpha_1 - \alpha_2$ is sufficiently small, Eq. (11) can be simplified by

$$\frac{\Delta V}{V} \approx \frac{\alpha_1 + \alpha_2}{2} \qquad (12)$$

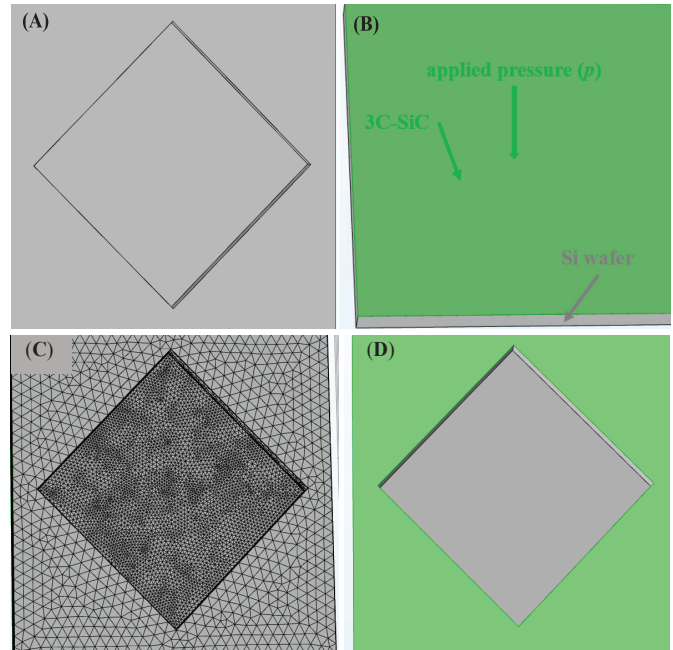## 2.4. Finite element simulation in COMSOL multiphysics

Fig. 3. (A) Proposed rotated square structures; (B) materials settings for silicon, silicon carbide (3C-SiC), and applied pressure; (C) mesh settings; and (D) clamping boundary conditions used for FEM in COMSOL multiphysics [32].

In Fig. 3, the finite element method (FEM) model in COMSOL multiphysics [32] is employed to calculate the stress and strain on the square diaphragm of MEMS pressure sensors. The simulated FEM model for the square structure involves four steps to determine the stress in the MEMS pressure sensor. Initially, a square structure of the MEMS pressure sensor is proposed, as shown in Fig. 3A. Subsequently, a thin layer of 3C-SiC material is applied to the top of a Si (100) wafer, as depicted in Fig. 3B. The anisotropic properties of Si and 3C-SiC materials, detailed in Table 1, along with the geometric conditions listed in Table 2, are incorporated. Additionally, pressure (*p*) is applied to create stress distribution on the thin diaphragm. In the mesh setting, a tetrahedral mesh density with 1,468,130 elements is employed throughout the sensor structure. An extremely high mesh density is specifically designated for the thin diaphragm, where stress concentration occurs, as illustrated in Fig. 3C. The fourth step involves setting a clamping boundary for the substrate, as shown in Fig. 3D. Ultimately, the stress distributions are obtained by solving the 3D structure of MEMS pressure sensors in the stationary solver of the solid mechanics module in COMSOL multiphysics [32].

3. Results and discussion

Figure 4 presents the stress distributions of square and circular diaphragm structures of MEMS pressure sensors, plotted using FEM in COMSOL multiphysics [32]. The results indicate that maximum stress concentrates along the corners of the thin diaphragm and the thick substrate. The stress distribution of the square diaphragm (see Fig. 4A) is higher than that of the circular diaphragm (see Fig. 4B) for MEMS pressure sensor diaphragms, as demonstrated in Table 4. Furthermore, the stress distributions of 3C-SiC on Si diaphragms are considerably higher than those of Si diaphragms alone, as indicated in Table

Table 5. Resultant von Mises stress (σ_{mises}) for a square diaphragm of a MEMS piezoresistive pressure sensor with Si only and Si with 3C-SiC.

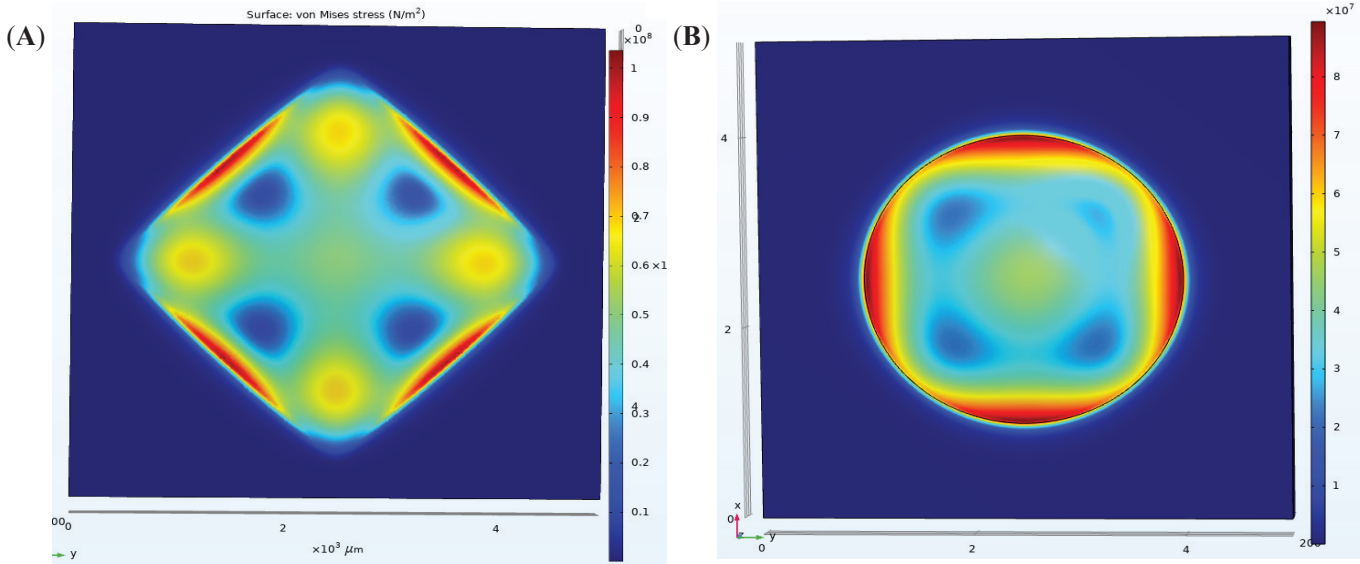| Geometries	Materials	von Mises stress (σ_{mises})
Square Diaphragm	Si	$\sigma_{mises} \cong 38.279$ (MPa)
	Si with 3C-SiC	$\sigma_{mises} \cong 95.579$ (MPa)
Circular Diaphragm	Si	$\sigma_{mises} \cong 28.678$ (MPa)
	Si with 3C-SiC	$\sigma_{mises} \cong 81.560$ (MPa)

Fig. 4. The von Mises stress distribution (σ_{mises}) for (A) square and (B) circular diaphragms for MEMS pressure sensors.

Table 4. Basic geometric and operating conditions used in COMSOL multiphysics [32].

Parameters	Name	Value
Wafer length Si (100)	L_w	5000 μm
Wafer thickness Si (100)	T_w	380 μm
Diaphragm length Si (100)	L_d	3000 μm
Diaphragm thickness Si (100)	T_d	50 μm
3C-SiC layer thickness	T_{3C-SiC}	500 nm
Applied pressure	p	50 kPa
Young's modulus of (100) Si	E_{Si}	130 GPa
Poisson's ratio of (100) Si	v_{Si}	0.28
Density of materials of (100) Si	ρ_{Si}	2330 kg/m³
Young's modulus of 3C-SiC	E_{SiC}	394 GPa
Poisson's ratio of 3C-SiC	v_{SiC}	0.25
Density of materials of 3C-SiC	ρ_{SiC}	3210 kg/m³
Elastic limit of Si	σ_{Si_limit}	180 MPa
Strain limit of Si	ε_{Si_limit}	1385 με
Elastic limit of 3C-SiC	σ_{SiC_limit}	1245 MPa
Strain limit of 3C-SiC	ε_{SiC_limit}	

5. Therefore, the principal stress distribution of the square structure of 3C-SiC on the Si diaphragm is investigated over a wide range of applied pressures (p) and diaphragm dimensions (i.e., length (L_d) and thickness (T_d)) to design for higher stress amplification in MEMS piezoresistive pressure sensors.

In Fig. 5, the principal stress (σ_{xy}) is plotted against the thickness (T_d) and length (L_d) of the diaphragm for varying applied pressures (p). Fig. 5A shows that the principal stress (σ_{xy}) increases significantly as the thickness (T_d) decreases. In Fig. 5B, the stress (σ_{xy}) increases as the length (L_d) increases and rises linearly with increasing pressure (p). Consequently, the stress distribution of MEMS pressure sensors can be significantly enhanced by increasing pressure, extending the length of the diaphragm, and reducing its thickness. Moreover, the elastic limit of 3C-SiC ($\sigma_{limit\_SiC} = 1245$ MPa) is listed in Table 2. The observed stress (σ) levels remain within the elastic limit of 3C-SiC materials, ensuring the safe operation of MEMS pressure sensors. Thus, the stress distribution in MEMS pressure sensors can be considerably amplified across a
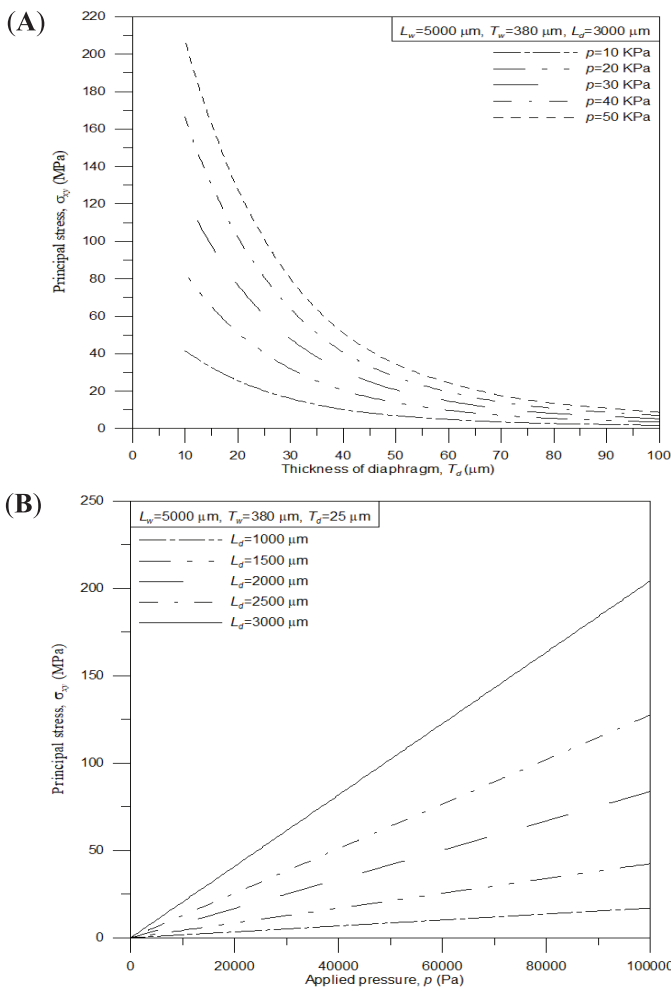
Fig. 5. Principle stress, σ_{xy} (MPa), versus (A) thickness of diaphragm (T_d) and (B) length of diaphragm (L_d) for different applied pressures (p) of MEMS pressure sensors.
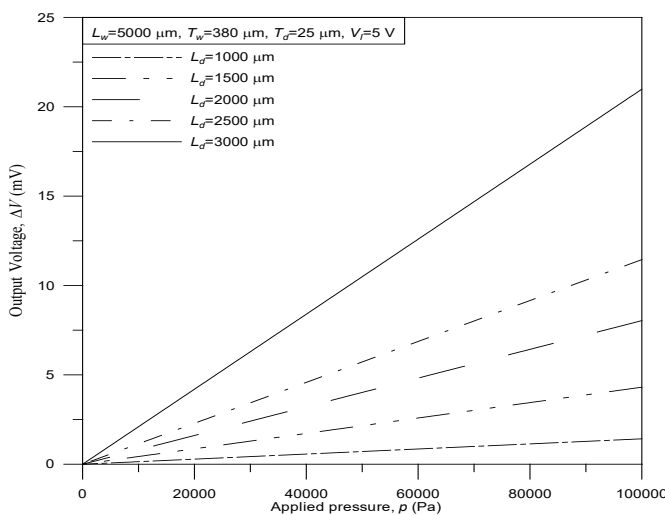

Fig. 6. Output voltage, ΔV (mV), versus applied pressure, p (Pa), for different diaphragm lengths (L_d) of MEMS pressure sensors.

wide range of diaphragm dimensions and pressure conditions.

In Fig. 6, the output voltage (ΔV) is calculated using Eq. (12) with varying applied pressure (p) for different lengths (L_d) of the diaphragm. The results indicate a linear increase in the output voltage (ΔV) as the pressure (p) rises. Additionally, there is an observed increase in the output voltage (ΔV) with an increase in the length (L_d) of the diaphragm. Consequently, a high output voltage (ΔV), exceeding 20 mV, can be achieved across a wide range of diaphragm lengths and thicknesses at an input voltage (V_I) of 5 V. Thus, the sensitivity of the MEMS piezoresistive pressure sensor, featuring a combination of a thin layer of 3C-SiC material on a Si diaphragm, can be significantly enhanced over a broad spectrum of diaphragm dimensions and pressure conditions.

4. Conclusions

This study has simulated and analysed the square diaphragm structure of a MEMS pressure sensor using 3D FEM in COMSOL multiphysics. A thin layer of 3C-SiC material, applied onto a Si diaphragm, enhances the stress distribution of MEMS pressure sensors. The stress distributions are calculated by solving the 3D structures of MEMS pressure sensors in the stationary solver of the solid mechanics module in COMSOL multiphysics. Notable results from this study include:

1. The stress distribution of the 3C-SiC material on a Si square diaphragm is considerably enhanced compared to that of a Si-only diaphragm for MEMS pressure sensors.

2. The stress distribution of the 3C-SiC material on a Si square diaphragm significantly increases under higher pressure, greater diaphragm length, and reduced diaphragm thickness. These stress values do not exceed the elastic limit of 3C-SiC materials. Hence, the stress distributions in MEMS pressure sensors with 3C-SiC on Si square diaphragms can be significantly amplified. An output voltage of more than 20 mV is achievable with this design. The results, demonstrating the utility of the thin layer of 3C-SiC material on a Si diaphragm, are pivotal for designing MEMS piezoresistive pressure sensors with enhanced stress amplification and robust performance, particularly in hazardous environments. Future work will involve the design and fabrication process of the 3C-SiC on Si square diaphragm for MEMS piezoresistive pressure sensors, employing MEMS technologies.

CRediT author statement

Nguyen Chi Cuong: Writing - Original draft preparation, Software; Trinh Xuan Thang: Conceptualisation, Methodology; Lam Minh Thinh, Vuong Dinh Duy Phuc: Investigation, Data curation; Truong Huu Ly: Software; Ngo Vo Ke Thanh, Le Quoc Cuong: Reviewing and Editing.

COMPETING INTERESTS

The authors declare that there is no conflict of interest regarding the publication of this article.

REFERENCES

[1] P. Song, Z. Ma, J. Ma, et al. (2020), "Recent progress of miniature MEMS pressure sensors", *Micromachines*, **11(1)**, DOI: 10.3390/mi11010056.

[2] H. Soy, İ. Toy (2021), "Design and implementation of smart pressure sensor for automotive applications", *Measurement*, **176**, DOI: 10.1016/j.measurement.2021.109184.

[3] Y. Kim, J.H. Oh (2020), "Recent progress in pressure sensors for wearable electronics: From design to applications", *Applied Sciences*, **10(18)**, DOI: 10.3390/app10186403.

[4] S.J. Prosser (1993), "Advances in sensors for aerospace applications", *Sensors and Actuators A: Physical*, **37-38**, pp.128-134, DOI: 10.1016/0924-4247(93)80024-B.

[5] C.S. Smith (1954), "Piezoresistance effect in germanium and silicon", *Physical Review Journals Archive*, **94(1)**, pp.42-49, DOI: 10.1103/PhysRev.94.42.

[6] P. Song, C. Si, M. Zhang, et al. (2020), "A novel piezoresistive MEMS pressure sensors based on temporary bonding technology", *Sensors*, **20(2)**, DOI: 10.3390/s20020337.

[7] V. Belwanshi (2021), "Analytical modeling to estimate the sensitivity of MEMS technology-based piezoresistive pressure sensor", *Journal of Computational Electronics*, **20**, pp.668-680, DOI: 10.1007/s10825-020-01592-5.

[8] P. Starr, K. Bartels, C.M. Agrawal, et al. (2016), "A thin-film pressure transducer for implantable and intravascular blood pressure sensing", *Sensors and Actuators A: Physical*, **248**, pp.38-45, DOI: 10.1016/j.sna.2016.06.035.

[9] J.W. Arkwright, I.D. Underhill, S.A. Maunder, et al. (2014), "Fiber optic pressure sensing arrays for monitoring horizontal and vertical pressures generated by traveling water waves", *IEEE Sensors Journal*, **14(8)**, pp.2739-2742, DOI: 10.1109/JSEN.2014.2311806.

[10] B. Morten, G.D. Cicco, M. Prudenziati (1992), "Resonant pressure sensor based on piezoelectric properties of ferroelectric thick films", *Sensors and Actuators A: Physical*, **31(1-3)**, pp.153-158, DOI: 10.1016/0924-4247(92)80096-L.

[11] M. Akiyama, Y. Morofuji, T. Kamohara, et al. (2006), "Flexible piezoelectric pressure sensors using oriented aluminum nitride thin films prepared on polyethylene terephthalate films", *Journal of Applied Physics*, **100(11)**, DOI: 10.1063/1.2401312.

[12] J.C. Suhling, R.C. Jaeger (2001), "Silicon piezoresistive stress sensors and their application in electronic packaging", *IEEE Sensors Journal*, **1(1)**, pp.14-30.

[13] K. Rajanna, S. Mohan (1987), "Longitudinal and transverse strain sensitivity of gold film", *Journal of Materials Science Letters*, **6**, pp.1027-1029, DOI: 10.1007/BF01729121.

[14] K. Rajanna, S. Mohan (1988), "Studies on meandering path thin film strain gage", *Sensors and Actuators*, **15(3)**, pp.297-303, DOI: 10.1016/0250-6874(88)87018-5.

[15] K. Rajanna, S. Mohan (1989), "Strain sensitive property of vacuum evaporated manganese films", *Thin Solid Films*, **172(1)**, pp.45-50, DOI: 10.1016/0040-6090(89)90116-8.

[16] S. Sanpath, V. Ramanaiah (1986), "Behavior of Bi-Sb alloy thin films as strain gages", *Thin Solid Films*, **137(2)**, pp.199-205, DOI: 10.1016/0040-6090(86)90020-9.

[17] G.R. Witt (1972), "Some effects of strain and temperature on the resistance of thin gold-glass cermet films", *Thin Solid Film*, **13(1)**, pp.109-115, DOI: 10.1016/0040-6090(72)90163-0.

[18] M. Hrovat, J. Holc, Z. Samardzija, et al. (2001), "The influence of firing temperature on gauge factors and the electrical and microstructural characteristics of thick-film resistor", *Journal of Materials Science Letters*, **20**, pp.701-705, DOI: 10.1023/A:1010954823442.

[19] K.J. Suja, E.S. Raveendran, R. Komaragiri (2013), "Investigation on better sensitive silicon based MEMS pressure sensor for high pressure measurement", *International Journal of Computers and Applications*, **72(8)**, pp.40-47.

[20] V. Belwanshi, S. Philip, A. Topkar (2022a), "Performance Study of MEMS piezoresistive pressure sensors at elevated temperatures", *IEEE Sensors Journal*, **22(10)**, pp.9313-9320, DOI: 10.1109/JSEN.2022.3164435.

[21] S.S. Kumar, B.D. Pant (2015), "Polysilicon thin film piezoresistive pressure microsensor: Design, fabrication and characterization", *Microsystem Technology*, **21**, pp.1949-1958, DOI: 10.1007/s00542-014-2318-1.

[22] P. Verma, D. Punetha, S.K. Pandey (2020), "Sensitivity optimization of MEMS based piezoresistive pressure sensor for harsh environment", *Silicon*, **12**, pp.2663-2671, DOI: 10.1007/s12633-019-00362-8.

[23] S.K. Jindal, S.P. Magam, M. Shaklya (2018), "Analytical modeling and simulation of MEMS piezoresistive pressure sensors with a square silicon carbide diaphragm as the primary sensing element under different loading conditions", *Journal of Computational Electronics*, **17**, pp.1780-1789, DOI: 10.1007/s10825-018-1223-8.

[24] M. Nag, J. Singh, A. Kumar, et al. (2019), "Sensitivity enhancement and temperature compatibility of graphene piezoresistive MEMS pressure sensor", *Microsystem Technologies*, **25**, pp.3977-3982, DOI: 10.1007/s00542-019-04392-5.

[25] V. Belwanshi, A. Topkar (2022b), "Quantitative analysis of MEMS piezoresistive pressure sensors based on wide band gap materials", *IETE Journal of Research*, **68(1)**, pp.667-677, DOI: 10.1080/03772063.2019.1620641.

[26] S. Li, Z. Zhang, J. Tang, et al. (2013), "A novel signal conditioning circuit for piezoresistive pressure sensor", *Unifying Electrical Engineering and Electronics Engineering*, **238**, pp.1707-1713, DOI: 10.1007/978-1-4614-4981-2_187.

[27] L. Jiang, R. Cheung (2009), "A review of silicon carbide development in MEMS applications", *Int. J. Computational Materials Science and Surface Engineering*, **2(3-4)**, pp.297-299, DOI: 10.1504/IJCMSSE.2009.027484.

[28] V. Belwanshi, A. Topkar (2019), "Design optimization and simulation of a diamond based piezoresistive pressure sensor for high temperature application", *Materials Today Proceedings*, **18**, pp.1017-1024, DOI: 10.1016/j.matpr.2019.06.542.

[29] V. Belwanshi, A. Topkar (2017), "Quantitative analysis of temperature effect on SOI piezoresistive pressure sensors", *Microsystem Technologies*, **23**, pp.2719-2725, DOI: 10.1007/s00542-016-3102-1.

[30] R. Khakpour, S.R.M. Mansouri, A.R. Bahadorimehr (2010), "Analytical comparison for square, rectangular and circular diaphragms in MEMS applications", *International Conference on Electronic Devices, Systems and Applications*, DOI: 10.1109/ICEDSA.2010.5503057.

[31] K.Y. Madhavi, K.A. Sumithradevi, M. Krishna, et al. (2011), "Analysis of square and circular diaphragms for a MEMS pressure sensor using a data mining tool", *International Conference on Electronic Devices, Systems and Applications*, DOI: 10.1109/CSNT.2011.63.

[32] COMSOL (2022), *COMSOL Multiphysics® 6.0 Release Highlights,* "MEMS module updates", https://www.comsol.com/, accessed 20 February 2023.

[33] M. Bao (2010), *Analysis and Design Principles of MEMS Devices*, Elsevier, 311pp.

[34] M.A. Hopcroft, W.D Nix, T.W Kenny, et al. (2010), "What is the Young's modulus of Silicon?", *Journal of Microelectromechanical Systems*, **19(2)**, pp.229-238, DOI: 10.1109/JMEMS.2009.2039697.

[35] P. Djemia, Y. Roussigné, G.F. Dirras, et al. (2004), "Elastic properties of β-SiC films by Brillouin light scattering", *Journal of Applied Physics*, **95(2)**, pp.2324-2330, DOI: 10.1063/1.1642281.

[36] P.H. Phan, D.V. Dao, K. Nakamura, et al (2015), "The piezoresistive effect of sic for MEMS sensors at high temperatures: A review", *Journal of Microelectromechanical Systems*, **24(6)**, pp.1663-1677, DOI: 10.1109/JMEMS.2015.2470132.

[37] M. Olszacki (2009), *Mod´Elisation Et Optimisation De Capteurs De Pression Pi´Ezor´Esistifs*, Ph.D. Thesis, INSA de Toulouse.